Transport and retention modeling of the liquid phase through a stratified porous leach-bed. Application for solid-state anaerobic co-digestion of cattle manure and roadside grass

A. Coutu, L. André, S. Guérin, V. Rocher, A. Pauss, T. Ribeiro

Transport and retention modelling of the liquid phase through a stratified porous leach-bed. Application for solid-state anaerobic co-digestion of cattle manure and roadside grass

A. Coutu[a], L. André[a], S. Guérin[b], V. Rocher[b], A. Pauss[c], T. Ribeiro[a*]

[a]Institut Polytechnique UniLaSalle, Université d'Artois, ULR 7519, 19 Rue Pierre Waguet, BP 30313, 60026 Beauvais, France.

[b]Direction Innovation SIAAP – Service public pour l'assainissement francilien, 82 avenue Kléber 92 700 Colombes, France.

[c]Université de Technologie de Compiègne, ESCOM, TIMR (Integrated Transformations of Renewable Matter), Centre de recherche Royallieu - CS 60 319 - 60 203 Compiègne Cedex.

*Corresponding author: Thierry Ribeiro; Tel.: +33 (0) 344 06 76 11; E-mail: thierry.ribeiro@unilasalle.fr

Abstract

The recirculation flow inside the leach-bed during solid-state anaerobic co-digestion of layered cattle manure and roadside grass was characterized using three different methods on lab scale reactors. Tracing experiments and method of moments were used to characterize percolation flow properties with different leach-bed compositions and a new criterion was proposed to quantitatively evaluate the ratio between preferential pathways and dead volumes for each experiment. The impact of recirculation flow on leach-bed complexity for different moments of SS-AD and substrate layering was characterized using steady-state reactor modelling and the impact of recirculation flow on microporosity and macroporosity evolutions all along SS-AD was determined using modelling of hydrodispersive parameters. It appeared that layering and time could significantly impact percolation flow and leach-bed complexity, until 36% of residence time variation and 110% of leach-bed complexity. Moreover, layering could impose a different percolation flow for each layer and cause a preferential pathways disruption.

Keywords

Residence time distribution; Percolation; Co-digestion; Biogas; Layering

1 Introduction

Since 2020, the availability of renewable energies became critical. Even while economies bent under the Covid-19 lockdowns, the price of fossil natural resources reached a record threshold (EBA, 2021). Additionally, methane emissions are the second-largest cause of global warming today. Oil and gas operations from the energy sector represented 76 Mt of methane emissions and the coal operations around 41 Mt (IEA, 2021). An available renewable energy to decrease these emissions is anaerobic digestion (AD). This process is a simple and efficient way to convert organic wastes into renewable energy as biogas. This gas can be valorized by gas injection or cogeneration of heat and electricity. This process also produces digestate that may substitute chemical fertilizers (Rocamora et al., 2020). AD contributes to bioeconomy reducing waste locally, supporting clean mobility and providing a clean and affordable energy. In Europe, 350 municipalities are producing biogas from their waste and 191 TWh of biogas were produced in 2020, representing 4.6% of the total gas consumption (EBA, 2021).

The solid-state anaerobic digestion (SS-AD) is defined by a total solid content higher than 15% (Rocamora et al., 2020; André et al., 2018; Degueurce et al., 2016) which is higher than conventional wet AD. SS-AD allows a higher volumetric production rate (Karthikeyan and Visvanathan, 2013; Brummeler et al., 2000) reducing the water use. However, numerous scientific and technological hurdles are limiting the process of development (André et al., 2018). Among these hurdles, this process reduces available free water within the leach-bed making it complicated to use mechanical mixing parts (Shewani et al., 2018). This is why most of the SS-AD processes work in batch mode, and mixing is provided by liquid phase recirculation from the bottom to the top of the reactor (Michele et al., 2015). However, this practice induces porosity evolution, which is a physical phenomenon due

47 to leach-bed heterogeneity and substrate degradation during anaerobic digestion. This modification
48 of the SS-AD leach-bed may lead to percolation difficulties and flow defects such as preferential
49 pathways and dead volumes, in which it is possible to observe partial substrate degradation resulting
50 in methane yield and cost losses (Hernandez-Shek et al., 2022; André et al., 2015). This variation in
51 the characteristics of the SS-AD leach-bed over time has already been observed by residence time
52 distribution experiments and modeling of macroporosity and microporosity evolution all along SS-
53 AD. Other investigations were done to optimize the impact on the recirculation strategy during SS-
54 AD studying feedstock and inoculum ratio (Dastyar et al., 2021), inoculation strategies (Meng et al.,
55 2019), or recirculation frequency (Coutu et al., 2022a; Qin et al., 2019; Pezzolla et al., 2017;
56 Degueurce et al., 2016) but there is very little work done regarding how recirculation flow impacts
57 the leach-bed properties during solid-state anaerobic co-digestion.

58 The main observed consequence of a recirculation flow inside a SS-AD leach-bed reactor is the
59 percolation quality which could impact the methane yield in the end. Percolation inside a SS-AD
60 leach-bed reactor is a phenomenon which can be compared to natural soil percolation. In fact, a
61 natural soil is a solid porous medium which is heterogeneous and contains preferential pathways
62 because of cracks, structural peds and wormholes and root channels (Beven and Germann, 1982).
63 Macropore and micropore distribution may be responsible for flow defects (Haws et al., 2004;
64 Larsson et al., 1999) and impacts the solute transport through the leach-bed (Haws et al., 2004;
65 Allaire-Leung et al., 2000; Gupta et al., 1999). Modeling makes it possible to characterize percolation
66 flow and solute transport. It is evidence that flow and transport processes in heterogeneous solid
67 porous medium cannot be described using classical models assuming uniform flow and transport
68 (Šimůnek and van Genuchten, 2008) and usual measurements may not be exploitable (Köhne, 2005).
69 Several conceptual approaches with various degrees of complexity and dimensionality have been
70 developed to modeling disequilibrium flow effect on solute transport (Lamy et al., 2009; Köhne et

al., 2009; Šimůnek and van Genuchten, 2008). One of the most used in the literature is the mobile-immobile (MIM) water model which was already used for SS-AD of cattle manure with different approaches (Coutu et al., 2022b; Shewani et al., 2015; André et al., 2015). However, there are still too few works proposing methods to characterize how recirculation flow impacts the leach-bed properties during solid-state anaerobic co-digestion.

The objectives were to (1) characterize the recirculation flow inside the leach-bed during anaerobic co-digestion of layered cattle manure and roadside grass; (2) determine the impact of recirculation flow on leach-bed complexity and substrate layering for different moments of SS-AD (after 0, 15 and 30 days); and (3) determine the impact of recirculation flow on microporosity and macroporosity evolution all along SS-AD.

2 Materials and methods

2.1 Characteristics of substrates and inoculum used

Two substrates were used for this study: cattle manure (CM) and roadside grass (RG). CM was sampled from the farm of the UniLaSalle Polytechnic Institute (Beauvais, France) according to the sampling plan described by the quartering method. Elementary samples were grouped, mixed and divided into four parts. Two opposing parts were eliminated and the remaining two parts were shuffled again. CM was chosen as the substrate to compare obtained results in literature concerning hydrodynamic parameters (André et al., 2015). RG was sampled with the same method after mowing the grass (Les Clayes-sous-Bois, France). RG had a particle size between 3 cm and 10 cm. CM and RG did not undergo any preliminary treatment as crushing or drying and the liquid part of the manure (LM) was used as the *inoculum* to bring the microbial consortium.

92 *2.2 Analytical methods*

93 The total solid content (TS) and the volatile content (VS) were respectively determined by a 105°C
94 drying for 24h and a combustion at 550°C for 2h (APHA, 1998) for each substrate and *inoculum*. pH
95 of the *inoculum* was determined using a pH meter (Mettler Toledo, Switzerland), the ratio between
96 total volatile fatty acid content (VFA) and the buffer capacity was determined by two titrations at
97 pH=4.4 and pH=5 using sulfuric acid with an automatic titrator (Mettler Toledo, Switzerland). Finally,
98 the Biochemical Methane Potential (BMP) was determined by the AMPTS system (Automatic
99 Methane Potential Test System, Bioprocess Control, Sweden) according to Holliger et al. (2016). All
100 analyses were carried out in triplicate. These tests were conducted at the beginning of experiments
101 and results are shown in **Table 1**.

102 *2.3 Experimental set-up*

103 *2.3.1 Solid-state anaerobic digestion at lab scale*

104 Leach-bed reactors (LBR) used were the same practical tool used in Coutu et al. (2020) to study solid-
105 state anaerobic digestion at lab scale through numerous experiments. Nine LBR were used for AD
106 monitoring initially filled with 200 g of solid substrates with different compositions ensuring the
107 same bulk density for each experiment and a correct percolation through the leach bed. Three
108 different mass compositions of raw substrates were studied in triplicate for the mixture CM/RG: 25
109 %, 50 % and 75 % of RG. 1 L of LM was added in each LBR to bring microbial consortium. Two different
110 types of experiments were led: a SS-AD experiment was coupled with a tracing experiment inside
111 the leach bed to perform a residence time distribution at different periods of AD. For each condition,
112 two LBR were stopped after 15 days and two LBR were stopped after 30 days to realize tracing
113 experiments and analytical measurements. Also, each LBR was used as the reactor and tracing
114 column. Extruded polystyrene discs were used to adjust the experimental height at 8 cm and

115 effective volume at 1.41 L for each reactor. During AD, substrates used were fully immersed inside
116 liquid phase and a stainless-steel aperture grid was placed below the leach bed to avoid any pump
117 clogging or accumulation of matter in pipes. A peristaltic pump was used on each LBR to recirculate
118 0.62 L of the liquid phase from the bottom to the top of the leach bed once a day, five a week. This
119 recirculation volume was arbitrarily chosen and represented 2/3 of the total liquid volume. Biogas
120 production was daily recorded with manual gas counters as described by Coutu et al. (2020), its
121 composition was analyzed by a gas chromatography (MicroGC, SRA Agilent 3000A) to measure
122 methane, carbon dioxide, nitrogen and hydrogen. At the beginning of SS-AD, the liquid phase was
123 fully recirculated once. For each LBR, RG was placed above CM creating a 2-layer stratification. This
124 structure was chosen to avoid possible inhibitions during SS-AD (André et al., 2019) and study the
125 impact of layering on residence time distribution. All the SS-AD system is represented **Fig 1**.

126 *2.3.2 Tracing experiments*

127 LBR were also used as tracing columns due to its cylindrical shapes. Tracer used should not be
128 absorbed or adsorbed by the leach bed during tracing experiments and should be easy to detect.
129 Preliminary experiments demonstrated that sodium chloride (NaCl) is not adapted when RG is one
130 of the studied substrates. In literature potassium bromide (KBr) is frequently used for tracing
131 experiments, particularly for soil hydrodynamics experiments (Lamy et al., 2009). Furthermore, KBr
132 is not expensive and the more conservative tracer in municipal solid waste (Woodman et al., 2015).
133 After several preliminary tests, KBr was validated for tracing experiments on CM and RG.

134 First, the tracing column studied was saturated with tap water at the same flow rate as SS-AD
135 conditions: 1.62 $L.min^{-1}$. A conductivity meter was placed at the LBR outlet to measure the
136 conductivity of water passing through the leach bed. Then the LBR was washed until reaching a stable
137 conductivity signal (between 660 $\mu S.cm^{-1}$ and 705 $\mu S.cm^{-1}$). After the washing step, 0.01 $mol.L^{-1}$ KBr
138 tracer solution with a 10,500 $\mu S.cm^{-1}$ conductivity was injected at constant flow during 20 s

139 respecting a Heaviside function. Then water was injected to elute the tracer and conductivity signal
140 was recorded with a RS232 data logger software (Eltima Software 2.7) each second as a function of
141 time until conductivity signal has returned to its initial value. The relative tracer concentration
142 between time-dependent concentration and initial tracer concentration (C/C_0) was obtained from
143 the ratio between measured conductivity and initial tracer conductivity, as described by André et al.
144 (2015). Tracing experiments were done in duplicate at the beginning of SS-AD, after 15 days and
145 after 32 days for each sacrificial LBR with 25%, 50% and 75% RG composition. Supplementary tracing
146 experiments were done at the beginning of SS-AD for 100% CM, 100% RG and 50% RG with a parallel
147 layering to highlight the layering impact on tracing experiments.

148 *2.4 Transport and retention characterization and modeling*

149 The more homogeneous over time the percolation flow, the more symmetrical the elution curve
150 (Sardin et al., 1991). This behavior is usually observed for homogeneous mediums like sands used in
151 soil hydrodynamics studies (Lamy et al., 2009). Conversely, the more heterogeneous over the
152 percolation flow, the more unsymmetrical the elution curve. Two main phenomena cause a
153 heterogeneous flow over time: the presence of preferential pathways and the presence of dead
154 volumes. Preferential pathways have a significant impact on the percolation flow when the
155 increasing part of the elution curve is steeper than the decreasing part of the elution curve and vice
156 versa for dead volumes. These phenomena are the first flow characterization to do.

157 *2.4.1 Flow characterization with residence time distribution*

158 The method of moments was used to determine the tracing experiment parameters. This method
159 allowed to characterize the recirculation flow inside the leach-bed during anaerobic co-digestion of
160 the 2 studied substrates. Zero, first and second order temporal moments described in (1) were used
161 to estimate the tracer mass balance, the mean residence time and the elution curve variance.

$$\mu_n = \int_0^{+\infty} t^n \frac{C(t)}{C_0} dt \quad \textbf{(1)}$$

With μ_n the n-order temporal moment and t the time (min). The ratio between mean residence time and geometrical residence time corresponds to the retardation factor R described in (2). This factor is equal to 1 when there are no leach bed interactions on the tracer. A retardation factor higher than 1 suggests the presence of liquid phase dead volumes and a retardation factor shorter than 1 suggests the presence of liquid phase preferential pathways.

$$R = \frac{\tau}{\tau_G}, \tau_G = \frac{V}{Q} \quad \textbf{(2)}$$

With R the retardation factor (dimensionless), τ the mean residence time (s), τ_G the geometrical residence time (s), and V the volume (m^3). Comparison of these different parameters between experiments allowed to evaluate percolation efficiency: a higher mean residence time means more water retention through the leach-bed, and higher retardation factor means a higher dispersive phenomenon. These behaviors are usually due to the presence of preferential pathways and dead volumes inside the solid porous medium.

2.4.2 Steady-state reactor analysis

Flow characterization obtained from elution curves allowed to model each tracing experiment with 2 classical steady-state process engineering models. These models were chosen because they are the more usual and theoretical models used in process engineering. This modeling allowed to characterize and compare the leach-bed complexity and thus the flow failures among each experiment for different moments of SS-AD.

- A cascade of continuous stirred tank reactors (CSTR):

From experimental elution curve, an equivalent elution curve with a cascade of CSTR was modeled from the mass balance of each LBR. A transfer function was also obtained and compared with experimental elution curve. The equation (3) (Houzelot, 2013) describes the elution curve modeled on the number of CSTR, N, and the mean residence time, τ. N is determined to approach the experimental curve.

$$E(t) = \left(\frac{N}{\tau}\right)^{N} . t^{N-1} . \frac{e^{-\frac{Nt}{\tau}}}{(N-1)!} \quad \textbf{(3)}$$

This modeling allowed to quantify a number of homogeneous layers represented by the number N, by informing the leach bed complexity.

- A plug-flow reactor with axial dispersion:

A Peclet criterium was determined to consider the asymmetry of residence time distribution and model the plug-flow reactor elution curve. It could be calculated from residence time distribution and elution curve variance as described in (4) assuming that convective flow is prevailing on diffusive flow. The plug-flow reactor with axial dispersion model is described in (5) (Houzelot, 2013). The elution curves were compared to these modeling to characterize the leach-bed complexity and the flow properties.

$$Pe = \frac{qL}{D} = 2\left(\frac{\tau}{\sigma}\right)^{2} \quad \textbf{(4)}$$

$$E(t) = \frac{1}{2}\left(\frac{Pe}{\pi\tau t}\right)^{\frac{1}{2}} . e^{\frac{Pe(\tau-t)^2}{4\tau t}} \quad \textbf{(5)}$$

2.4.3 Comparative flow criterion

A criterion was proposed and calculated from elution curves. This criterion allows to quantitatively evaluate the ratio between preferential pathways and dead volumes for each experiment. PP (for

197 preferential pathways) was determined to calculate the elution curve integral between the
198 beginning of the tracing experiment and the mean residence time. The DV (for dead volumes) was
199 determined to calculate the elution curve integral between the mean residence time and the end of
200 tracing experiments. The ratio PP/DV provides a dimensionless value, easy to understand and which
201 could be compared to each next experiment in the literature. PP and DV expressions are detailed in
202 equations (6) and (7), where E(t) is the zero-order temporal moment given by (1) These equations
203 must respect that the sum between PP and DV is equal to 1 to respect the tracer mass balance.

$$PP = \int_0^{\tau} E(t)dt \quad \textbf{(6)}$$

$$\mathrm{DV} = \int_{\tau}^{+\infty} E(t)dt \quad \textbf{(7)}$$

204

205 *2.4.4 Modelling of hydrodispersive parameters*

206 Modelling of hydrodispersive parameters allowed to determine the impact of recirculation flow on
207 microporosity and macroporosity evolution all along SS-AD. Identification of hydrodispersive
208 parameters was done on elution curves obtained from tracing experiments. These parameters could
209 be read in conjunction with steady-state models and retardation factor to realize a complete flow
210 characterization. A two-region model also known as MIM model (Mobile-Immobile water) was used
211 to identify representative hydrodispersive parameters of the flow. The volumetric water content is
212 assumed to be divided into 2 distinct regions in this model: the mobile region and the stagnant
213 region. The convective flow is assumed occurring in the mobile region only and tracer exchange rate
214 is supposed following a first-order kinetics (Lamy et al., 2009; Šimůnek and van Genuchten, 2008;
215 van Genuchten and Wieranga, 1976). The representative equations are described in (8) where θ_m
216 and θ_{im} are the fractions of solid matter filled with mobile and stagnant water ($m^3_{tracer}.m^{-3}$), C_m and

217 C_{im} are the tracer concentrations in mobile and stagnant regions (kg.m^{-3}), D_m is the diffusive
218 coefficient (m^2.h^{-1}), q is the Darcian velocity (m.h^{-1}) and α is the tracer exchange rate between mobile
219 and stagnant regions (h^{-1}).

$$\begin{cases} \theta_m \frac{\partial C_m}{\partial t} = \theta_m D_m \frac{\partial^2 C_m}{\partial z^2} - q \frac{\partial C_m}{\partial z} - \alpha(C_m - C_{im}) \\ \theta_{im} \frac{\partial C_{im}}{\partial t} = \alpha(C_m - C_{im}) \end{cases} \quad \textbf{(8)}$$

220 The hydrodispersive parameters to be determined were θ_{im} and α. These parameters were obtained
221 using HYDRUS-1D software which found the best fit between the MIM-model and the experimental
222 elution curve (Šimůnek and van Genuchten, 2008). The input parameters are the total volumetric
223 content, the length of studied leach bed L, the total dry bulk density θ, the pulse duration t_{pulse} of
224 the tracer injection and the Darcian velocity q.

225 ## 3 Results and discussion

226 ### *3.1 Anaerobic digestion performances*

227 Tracing experiments were realized before SS-AD, after 15 days and 30 days of SS-AD. During this
228 process, each duplicate had the same behavior even if the technology used for gas counters may
229 introduce some uncertainty on the methane flow measurement (20 mL per measurement). The
230 higher the RG leach-bed composition, the higher the methane production rate. This observation was
231 consistent with BMP results which highlighted a higher methane yield for RG than CM. Mass balances
232 ranged from 96.11 % to 98.56 % ensuring there was no gas leakage and VS removal was measured
233 on each leach bed and represented between 54.9 % and 69.3 % of substrate degradation. At the end
234 of each experiment, pH reached a value between 7.9 and 8.0, attesting an appropriate balance
235 between VFA production and substrate degradation during SS-AD process. The maximum methane
236 production rate obtained during these experiments reached 75% to 95 % of BMP made depending

237 on the RG proportion. These deviations could be explained by the manure flotation and the reduced
238 accessibility of the substrates compared to BMP conditions. The cumulated methane yield is
239 represented in **Fig 2**. These data clearly have shown that the SS-AD experiments were held without
240 inhibitions but substrate degradation was partial for each experiment. This difference of production
241 rates between BMP values and experimental measures have shown the leach-bed layering impact
242 and percolation problems on methane production. Approximately two third of organic matter was
243 not accessible. This observation was indicative of a complex solid matrix, which could be explained
244 by the presence of numerous preferential pathways and dead volumes within the leach bed. These
245 observations justified the need to investigate this phenomenon through adapted tools.

246 *3.2 Tracer elution curves obtained in saturated conditions*

247 The elution curves were studied through a residence time distribution, giving a lot of information
248 about percolation characteristics of the liquid phase through the leach bed and more globally about
249 SS-AD recirculating process. The more symmetric the curve shape, the more ideal the flow.

250 *3.2.1 Elution curves before AD*

251 The elution curves obtained before SS-AD provided a lot of information concerning percolation
252 characteristics of the liquid phase through the leach-bed. These curves are represented in **Fig 3** as a
253 function of time and **Fig 4** as a function of substrate compositions. First of all, tracer mass balances
254 were respected with a value between 89.8 % and 99.7 %. These mass balance variations were
255 probably due to retention volumes inside the leach-bed where the tracer stayed trapped. At
256 equivalent density, the leach-bed only composed with RG provided an elution curve which was less
257 spread over time than the leach-bed only composed with CM. This could be explained by a faster
258 percolation flow and a lower dispersive phenomenon inside the leach-bed composed with RG than
259 the leach-bed composed with CM. Mixes composed of 25 % RG and 75 % CM and 75 % RG and 25 %

CM showed that the higher the RG composition, the closer the observed flow to that observed for pure RG: dispersive phenomenon decreased and percolation flow was faster as represented in **Fig 3** (A). However, the behavior of the mix composed of 50 % of RG and 50 % of CM was completely different: the percolation flow was much slower than others observed leach-bed. Other observations during SS-AD showed the same phenomenon. When the compositions of each substrate approached 50%, the percolation flow became different for each layer. This means that tracer flow inside the tracing column became heterogeneous over time, resulting in a drop-in flow velocity and a non-negligible increasing of the dispersive phenomenon. This behavior had already been observed in hydrogeology studies (Lamy et al., 2009).

3.2.2 Elution curves during AD

All along SS-AD process, Elution curves had a tracer concentration peak which appeared earlier and less spread out. This means a higher recirculation flow inside the leach-bed and a decrease of diffusive phenomena, as observed by André et al. (2015): the more degraded the leach bed was, the more compacted it was. Macroporosity was decreasing to the benefit of microporosity, explaining the tracer diffusivity losses and preferential pathway formation on reactor sides due to the leach bed compaction. A second phenomenon appeared when CM and RG compositions were close enough during codigestion: the elution curve had a bimodal shape as represented in **Fig 3** (B and C) and **Fig 4** (B). These curve shapes demonstrated the existence of two different flow regions contributing to diffusive and dispersive transfer mechanisms. In these different experiments, the 2-layers horizontal layering created a separation between the two substrates. This separation between the two substrate layers probably applied preferential pathway disruption which had the effect of a local homogenization directly inducing a modification of the elution curve shape.

3.2.3 Layering impact on residence time distribution

Another tracing experiment was done before SS-AD with the mix composed of 50 % of CM and 50 % of RG respecting two different spatial configurations: a serial layer tracing experiments (SLTE) and a parallel layer's tracing experiments (PLTE) for each substrate. Obtained elution curves are illustrated in **Fig 3** (D). The two experiments provided very different behaviors. The PLTE showed more preferential pathways and less tracer dispersion inside the leach-bed contrary to SLTE that showed less preferential pathways and more tracer dispersion. These observations could mean that the parallel layers disposing allow making the preferential pathway disruption disappear. In this case, a preferential pathway may occur in the layer having the higher macroporosity.

3.3 Residence time distribution and flow characterization

The method of moments was used to determine the mean residence time and the retardation factor R for each studied composition all along SS-AD. Results are illustrated in **Fig 5** (A) and (B). The mean residence time was firstly determined and compared to geometrical residence time to obtain a retardation factor for each experiment respecting equation (2). First, it was noticeable that every retardation factor was higher than 1, which is consistent: the mean residence time was higher than the geometrical residence time, which meant a non-ideal flow percolation.

Results obtained corroborated precedent observations: before SS-AD, the higher the CM composition, the higher the observed retardation factor. That meant a leach-bed full of CM resulted in less preferential pathways and more dispersive phenomenon in comparison with RG at the same density. However, when RG and CM compositions were in the same range, mean residence time and retardation factor significantly increased. This phenomenon was probably due to a preferential pathways disruption as explained previously. During SS-AD, this observation reversed the more significant the substrate composition (close to 50 %), the lower the mean residence time and the

retardation factor observed. The tracer percolation through the leach-bed was modified as a function of time and this phenomenon was probably due to the solid porous medium degradation. This leach-bed modification resulted in a modification of preferential pathways and dead volumes inside the solid porous medium. There was also a different degradation kinetics for each substrate which led to a different flow characteristics evolution during SS-AD. During SS-AD, these results showed an increase in the proportion of dead volumes compared to preferential pathways higher for compositions close to 50 % for each substrate. At the end of SS-AD, the leach-bed retraction phenomenon suggested by André et al. (2015) could be observed in this study with the evolution of preferential pathways and dead volumes. The same behavior was observed between each composition before and after SS-AD: when the composition for each substrate was enough (close to 50 % in this study), more preferential pathways formed around the leach-bed and more dead volumes appeared inside the leach-bed.

3.4 Comparative flow criterion

The PP/DV ratio was determined for each experiment before and during SS-AD and is illustrated in **Fig 5 (C)**. This ratio was higher on CM than RG before SS-AD, which meant that the proportion of preferential pathways compared to dead volumes was higher in CM than RG before SS-AD. This result was linked with residence time and retardation factor values and previous conclusions. Moreover, the closer to 50 % substrate composition for each substrate, the higher the proportion of preferential pathways compared to dead volumes. During SS-AD, this ratio is balanced out between different compositions, probably because of the leach-bed homogenization. At the end of SS-AD, the behavior observed was completely different: the higher the proportion of RG, the higher the PP/DV ratio. This behavior could be explained by a higher density for RG than CM, causing a higher digestate compaction. Finally, for the 50 % RG and 50 % CM experiment, the PP/DV ratio was determined in parallel and serial layering. Results showed a decrease of preferential pathways and an increase of

329 dead volumes for a parallel layering. This ratio gave a similar conclusion than other tools for
330 hydrodynamics characterization and is more explicit than usual values as mean residence time
331 distribution and retardation factor. Moreover, this value could be directly compared with other
332 experiments in the literature due to their dimensionless nature.

333 *3.5 Steady-state reactor modeling*

334 Mean residence times and elution curves previously obtained from residence time distribution were
335 used to modelling equivalent flow of 2 ideal steady-state reactors: the cascade of continuous stirred
336 tank reactor and the plug-flow reactor with axial dispersion for each experiment. The percolation
337 flow observed was then compared to these ideal flows to characterize the leach-bed complexity. The
338 plug-flow reactor with axial dispersion modeling provided very different elution curves from
339 experimental results with larger mean residence times, larger retardation factors and a flattened
340 elution curve shape. This observation could be explained by a very different behavior between a
341 layered leach-bed and a plug-flow reactor. Therefore, the plug-flow reactor with axial dispersion
342 model is not adapted for layered leach-bed reactors. Using the cascade CSTR model, the
343 experimental elution curves were comparable with the modeled elution curves but a different
344 number of CSTR was found depending on the leach-bed complexity. This is why the equivalent CSTR
345 number was used as characterization parameters of the leach-bed complexity. All results are
346 presented in **Table 2**. A strong heterogeneity of each leach-bed was observed, with a higher
347 complexity for 2-layers leach-beds. This observation was coherent with the solid porous medium
348 composition: the more heterogeneous the leach-bed, the more heterogeneous the percolation flow
349 crossing it. Moreover, the flow heterogeneity increased during SS-AD and decreased at the end of
350 SS-AD. This last observation could be explained by the flow around the leach-bed observed in André
351 et al. (2015) and representing an observation bias due to leach-bed retraction. Finally, parallel
352 layering of CM and RG in a leach-bed composed of 50 % of RG and CM showed a higher heterogeneity

than serial layering. This result is coherent with previous observations and could be related to the equivalent resistance analogy, well known in fluid mechanics: percolation flow was different for each substrate inside the parallel layered leach-bed, causing a global percolation flow different from percolation flow for each substrate. This behavior could be explained by a different flow resistance for each substrate. This result could be a great solution to minimize percolation problems inside a leach-bed reducing flow resistance. However, this modification of layering could bring more flow defaults as non-desirable preferential pathways and dead volumes resulting in degradation heterogeneity and methane yield losses.

3.6 Hydrodispersive parameters identification

Hydrodispersive parameters modelling was done using Hydrus-1D. This software allows simulating percolation flow inside porous and incompressible mediums with solute transfer from an elution curve. The Richards' equation is solved to determine pressure, water content and hydraulic conductivity of the flow and different soils hydrodynamic models are available. This software is usually used for water and solute transfer experiments inside different soils (Torkzaban et al., 2008; Boivin et al., 2006; Abbasi et al., 2004) and recently used for SS-AD (Shewani et al., 2015; André et al., 2015). Some inlet parameters had to be specified to proceed: the height of the leach-bed, the saturated water content and the tracer injection time. Considering a saturated model (equation 8), the saturated water content is equal to the total water content in this study. The outlet parameters obtained were the fraction of solid matter filled with stagnant water representing the microporosity (θ_{im}) and the tracer exchange rate between mobile and stagnant regions (α). Results obtained after hydrodispersive simulations are illustrated in **Fig 6**. It could be observed that when RG composition was sufficiently low, microporosity (θ_{im}) highly increased throughout SS-AD and decreased at the end of SS-AD. This behavior is typical of SS-AD: as substrates are deteriorated through SS-AD, permeability decreased and porous medium became more compact and impermeable (André et al.,

2015). This phenomenon led to a fall in macroporosity and a leach-bed retraction (Shewani et al., 2015). However, at the end of SS-AD, the porous medium became completely impermeable and all the liquid phase percolated on the sides, which could be observed with an increase in macroporosity and a decrease in microporosity. When each substrate composition was high enough, a different behavior was observed: microporosity was higher at the beginning of SS-AD and decreased all along SS-AD. This phenomenon could be explained in this study by a more compact leach-bed layering with RG which fit in CM interstices, providing more complexity inside the porous medium and increasing the microporosity at the beginning of SS-AD. Then the permeability loss should decrease microporosity all along SS-AD. The MIM model used was useful to describe the porous medium hydrodynamics properties. One of the studied parameters of the model is the tracer exchange rate (α) between macroporosity and microporosity. The tracer exchange rate value highly increased when each substrate composition approximated 50 %. This phenomenon could be explained in this study by the same phenomenon described before: a more compact leach-bed layering with RG which fit in CM interstices, providing more exchanges between mobile and stagnant regions. The developed tools used in this study provided very interesting observations about recirculation impacts on SS-AD. However, tracing experiments are very dependent on the column size and geometry. The observations made during this study will be scaled for real full-scale reactors but geometric, dynamic and cinematic similarities should be respected.

4 Conclusions

The recirculation flow inside the leach-bed was characterized before and during SS-AD of layered cattle manure and roadside grass with different tools including a new comparative flow criterion: the PP/DV ratio. The impact of recirculation flow on leach-bed complexity was determined for different moments of SS-AD and incites changing recirculation strategy to minimize water and energy costs in the context of operating cost reduction. This study provided a complete method to

characterize recirculation flow during SS-AD, which could be continued for other substrates and experimental conditions and should be tested in pilot-scale conditions to observe the change of scale effect.

5 Acknowledgments

The authors gratefully thank the program MOCOPEE (www.mocopee.fr) and the FEDER fund (FEDER PO Picardie / MOCOPEE PI0012581) for the support provided for this work and the PhD grant of Arnaud Coutu. The authors want to thank also Edvina Lamy for her help and Pauline Louis for her carefully reading of the manuscript.

6 References

Abbasi, F., Feyen, J., van Genuchten, M.T., 2004. Two-dimensional simulation of water flow and solute transport below furrows: model calibration and validation. Journal of Hydrology 290, 63–79. https://doi.org/10.1016/j.jhydrol.2003.11.028

Allaire-Leung, S.E., Gupta, S.C., Moncrief, J.F., 2000. Water and solute movement in soil as influenced by macropore characteristics. 2. Macropore tortuosity. Journal of contaminant hydrology 41, 303–315. https://doi.org/10.1016/S0169-7722(99)00074-1

André, L., Durante, M., Pauss, A., Lespinard, O., Ribeiro, T., Lamy, E., 2015. Quantifying physical structure changes and non-uniform water flow in cattle manure during dry anaerobic digestion process at lab scale: Implication for biogas production. Bioresource Technology 192, 660–669. https://doi.org/10.1016/j.biortech.2015.06.022

André, L., Pauss, A., Ribeiro, T., 2018. Solid anaerobic digestion: State-of-art, scientific and technological hurdles. Bioresource Technology 247, 1027–1037. https://doi.org/10.1016/j.biortech.2017.09.003

André, L., Zdanevitch, I., Pineau, C., Lencauchez, J., Damiano, A., Pauss, A., Ribeiro, T., 2019. Dry anaerobic co-digestion of roadside grass and cattle manure at a 60 L batch pilot scale. Bioresource Technology 289, 121737. https://doi.org/10.1016/j.biortech.2019.121737

APHA, 1998. Standard Methods for the Examination of Water and Wastewater. American Public Health Association, 20th ed. American water works association and water environment federation, Washington, USA.

Beven, K., Germann, P., 1982. Macropores and water flow in soils. Water Resources Research 18, 1311–1325.

Boivin, A., Šimůnek, J., Schiavon, M., van Genuchten, M.T., 2006. Comparison of Pesticide Transport Processes in Three Tile-Drained Field Soils Using HYDRUS-2D. Vadose Zone Journal 5, 838–849. https://doi.org/10.2136/vzj2005.0089

Buchter, B., Hinz, C., Flury, M., Flühler, H., 1995. Heterogeneous Flow and Solute Transport in an Unsaturated Stony Soil Monolith. Soil Science Society of America Journal 59, 14–21. https://doi.org/10.2136/sssaj1995.03615995005900010002x

Coutu, A., André, L., Mottelet, S., Azimi, S., Guérin, S., Rocher, V., Pauss, A., Ribeiro, T., 2020. Conception de réacteurs et compteurs de gaz innovants pour la méthanisation en voie sèche à l'échelle laboratoire : Design of innovative reactors and gas counters for dry anaerobic digestion study at laboratory scale. TSM 71–82. https://doi.org/10.36904/tsm/202009071

Coutu, A., Mottelet, S., Guérin, S., Rocher, V., Pauss, A., Ribeiro, T., 2022a. Methane yield optimization using mix response design and bootstrapping : application to solid-state anaerobic co-digestion process of cattle manure and damp grass. Bioresource Technology Reports 17, 100883. https://doi.org/10.1016/j.biteb.2021.100883

Coutu, A., Hernández-Shek, M.A., Mottelet, S., Guérin, S., Rocher, V., Pauss, A., Ribeiro, T., 2022b. A coupling model for solid-state anaerobic digestion in leach-bed reactors: Mobile-Immobile water and anaerobic digestion model. Bioresource Technology Reports 100961. https://doi.org/10.1016/j.biteb.2022.100961

Dastyar, W., Mohammad Mirsoleimani Azizi, S., Dhadwal, M., Ranjan Dhar, B., 2021. High-solids anaerobic digestion of organic fraction of municipal solid waste: Effects of feedstock to inoculum ratio and percolate recirculation time. Bioresource Technology 337, 125335. https://doi.org/10.1016/j.biortech.2021.125335

Degueurce, A., Trémier, A., Peu, P., 2016. Dynamic effect of leachate recirculation on batch mode solid state anaerobic digestion: Influence of recirculated volume, leachate to substrate ratio and recirculation periodicity. Bioresource Technology 216, 553–561. https://doi.org/10.1016/j.biortech.2016.05.113

EBA, 2021. Annual statistical report of the European Biogas Association. European Overview 2021.

Feyen, J., Jacques, D., Timmerman, A., Vanderborght, J., 1998. Modelling Water Flow and Solute Transport in Heterogeneous Soils: A Review of Recent Approaches. Journal of Agricultural Engineering Research 70, 231–256. https://doi.org/10.1006/jaer.1998.0272

Gerke, H.H., van Genuchten, M.T., 1993. A dual-porosity model for simulating the preferential movement of water and solutes in structured porous media. Water Resources Research 29, 305–319. https://doi.org/10.1029/92WR02339

Gupta, A., Destouni, G., Jensen, M.B., 1999. Modelling tritium and phosphorus transport by preferential flow in structured soil. Journal of Contaminant Hydrology 35, 389–407. https://doi.org/10.1016/S0169-7722(98)00107-7

Gwo, J., Jardine, P., Wilson, G., Yeh, G., 1995. A multiple-pore-region concept to modeling mass transfer in subsurface media. Journal of Hydrology 164 (1–4), 217–237. https://doi.org/10.1016/0022-1694(94)02555-P

Hafner, S.D., Fruteau de Laclos, H., Koch, K., Holliger, C., 2020. Improving Inter-Laboratory Reproducibility in Measurement of Biochemical Methane Potential (BMP). Water 12, 1752. https://doi.org/10.3390/w12061752

Haws, N.W., Das, B.S., Rao, P.S.C., 2004. Dual-domain solute transfer and transport processes: evaluation in batch and transport experiments. J Contam Hydrol 75, 257–280. https://doi.org/10.1016/j.jconhyd.2004.07.001

Haws, N.W., Rao, P.S.C., Simunek, J., Poyer, I.C., 2005. Single-porosity and dual-porosity modeling of water flow and solute transport in subsurface-drained fields using effective field-scale parameters. Journal of Hydrology 313, 257–273. https://doi.org/10.1016/j.jhydrol.2005.03.035

Hernandez-Shek, M.A., Peultier, P., Pauss, A., Ribeiro, T., 2022. Rheological evolution of straw-cattle manure (SCM) treated by dry anaerobic digestion in batch and in continuous pilot reactors. Waste Management 144, 411–420. https://doi.org/10.1016/j.wasman.2022.04.014

Holliger, C., Alves, M., Andrade, D., Angelidaki, I., Astals, S., Baier, U., Bougrier, C., Buffière, P., Carballa, M., de Wilde, V., Ebertseder, F., Fernández, B., Ficara, E., Fotidis, I., Frigon, J.-C., de Laclos, H.F., Ghasimi, D.S.M., Hack, G., Hartel, M., Heerenklage, J., Horvath, I.S., Jenicek, P., Koch, K., Krautwald, J., Lizasoain, J., Liu, J., Mosberger, L., Nistor, M., Oechsner, H., Oliveira, J.V., Paterson, M., Pauss, A., Pommier, S., Porqueddu, I., Raposo, F., Ribeiro, T., Rüsch Pfund, F., Strömberg, S., Torrijos, M., van Eekert, M., van Lier, J., Wedwitschka, H., Wierinck, I., 2016. Towards a standardization of biomethane potential tests. Water Science and Technology 74, 2515–2522. https://doi.org/10.2166/wst.2016.336

Houzelot, J.-L., 2013. Distribution des temps de séjour et efficacité des réacteurs chimiques. Opérations unitaires. Génie de la réaction chimique. https://doi.org/10.51257/a-v1-j4014

IEA, 2021. Methane Emissions from Oil and Gas, International Energy Agency, Paris. https://www.iea.org/reports/methane-emissions-from-oil-and-gasMethane Emissions from Oil and Gas – International Energy Agency, Paris, 2021. IEA. URL https://www.iea.org/reports/methane-emissions-from-oil-and-gas (accessed 1.24.22).

Jury, W.A., Roth, K., 1990. Transfer functions and solute movement through soil: theory and applications. Birkhäuser Verlag, Basel; Boston.

Karthikeyan, O.P., Visvanathan, C., 2013. Bio-energy recovery from high-solid organic substrates by dry anaerobic bio-conversion processes: a review. Rev Environ Sci Biotechnol 12, 257–284. https://doi.org/10.1007/s11157-012-9304-9

496 Koch, K., Lippert, T., Drewes, J.E., 2017. The role of inoculum's origin on the methane yield of different substrates
497 in biochemical methane potential (BMP) tests. Bioresource Technology 243, 457–463.
498 https://doi.org/10.1016/j.biortech.2017.06.142

499 Köhne, J.M., 2005. Mini Suction Cups and Water-Extraction Effects on Preferential Solute Transport. Vadose Zone
500 Journal 4, 866–880. https://doi.org/10.2136/vzj2004.0111

501 Köhne, J.M., Köhne, S., Šimůnek, J., 2009. A review of model applications for structured soils: a) Water flow and
502 tracer transport. Journal of Contaminant Hydrology, Preferential Flow 104, 4–35.
503 https://doi.org/10.1016/j.jconhyd.2008.10.002

504 Lamy, E., Lassabatere, L., Bechet, B., Andrieu, H., 2009. Modeling the influence of an artificial macropore in sandy
505 columns on flow and solute transfer. Journal of Hydrology 376, 392–402.
506 https://doi.org/10.1016/j.jhydrol.2009.07.048

507 Larsson, M.H., Jarvis, N.J., Torstensson, G., Kasteel, R., 1999. Quantifying the impact of preferential flow on solute
508 transport to tile drains in a sandy field soil. Journal of Hydrology 215, 116–134.
509 https://doi.org/10.1016/S0022-1694(98)00265-0

510 Meng, L., Maruo, K., Xie, L., Riya, S., Terada, A., Hosomi, M., 2019. Comparison of leachate percolation and
511 immersion using different inoculation strategies in thermophilic solid-state anaerobic digestion of pig
512 urine and rice straw. Bioresource Technology 277, 216–220.
513 https://doi.org/10.1016/j.biortech.2019.01.011

514 Michele, P., Giuliana, D., Carlo, M., Sergio, S., Fabrizio, A., 2015. Optimization of solid state anaerobic digestion of
515 the OFMSW by digestate recirculation: A new approach. Waste Management 35, 111–118.
516 https://doi.org/10.1016/j.wasman.2014.09.009

517 Pezzolla, D., Di Maria, F., Zadra, C., Massaccesi, L., Sordi, A., Gigliotti, G., 2017. Optimization of solid-state
518 anaerobic digestion through the percolate recirculation. Biomass and Bioenergy 96, 112–118.
519 https://doi.org/10.1016/j.biombioe.2016.11.012

520 Qin, Y., Wu, J., Xiao, B., Cong, M., Hojo, T., Cheng, J., Li, Y.-Y., 2019. Strategy of adjusting recirculation ratio for
521 biohythane production via recirculated temperature-phased anaerobic digestion of food waste. Energy
522 179, 1235–1245. https://doi.org/10.1016/j.energy.2019.04.182

523 Rocamora Miguel, I., Bajón fernández, Y., Wagland, S., 2021. Use of Inoculum, Water and Percolate as Strategy to
524 Avoid Inhibition on Dry-Batch Anaerobic Digestion of Organic Fraction of Municipal Solid Waste.
525 https://doi.org/10.17862/cranfield.rd.15022206.v1

526 Rocamora, I., Wagland, S.T., Villa, R., Simpson, E.W., Fernández, O., Bajón-Fernández, Y., 2020. Dry anaerobic
527 digestion of organic waste: A review of operational parameters and their impact on process
528 performance. Bioresource Technology 299, 122681. https://doi.org/10.1016/j.biortech.2019.122681

Sardin, M., Schweich, D., Leij, F.J., van Genuchten, M.T., 1991. Modeling the Nonequilibrium Transport of Linearly Interacting Solutes in Porous Media: A Review. Water Resources Research 27, 2287–2307. https://doi.org/10.1029/91WR01034

Shewani, A., Horgue, P., Pommier, S., Debenest, G., Lefebvre, X., Gandon, E., Paul, E., 2015. Assessment of percolation through a solid leach bed in dry batch anaerobic digestion processes. Bioresource Technology 178, 209–216. https://doi.org/10.1016/j.biortech.2014.10.017

Shewani, A., Horgue, P., Pommier, S., Debenest, G., Lefebvre, X., Decremps, S., Paul, E., 2018. Assessment of Solute Transfer Between Static and Dynamic Water During Percolation Through a Solid Leach Bed in Dry Batch Anaerobic Digestion Processes. Waste Biomass Valor 9, 2081–2089. https://doi.org/10.1007/s12649-017-0011-1

Šimůnek, J., van Genuchten, M.T., 2008. Modeling Nonequilibrium Flow and Transport Processes Using HYDRUS. Vadose Zone Journal 7, 782–797. https://doi.org/10.2136/vzj2007.0074

ten Brummeler, E., 2000. Full scale experience with the BIOCEL process. Water Science and Technology 41, 299–304. https://doi.org/10.2166/wst.2000.0084

Torkzaban, S., Bradford, S.A., van Genuchten, M.Th., Walker, S.L., 2008. Colloid transport in unsaturated porous media: The role of water content and ionic strength on particle straining. Journal of Contaminant Hydrology 96, 113–127. https://doi.org/10.1016/j.jconhyd.2007.10.006

van Genuchten, M.Th., Wierenga, P.J., 1976. Mass transfer studies in sorbous porous media I. Analytical solutions. Soil Science Society of America Journal Vol 40.

Wang, B., Strömberg, S., Nges, I.A., Nistor, M., Liu, J., 2016. Impacts of inoculum pre-treatments on enzyme activity and biochemical methane potential. J Biosci Bioeng 121, 557–560. https://doi.org/10.1016/j.jbiosc.2015.10.004

Woodman, N.D., Rees-White, T.C., Stringfellow, A.M., Beaven, R.P., Hudson, A.P., 2015. Multiple-tracer tests for contaminant transport process identification in saturated municipal solid waste. Waste Management 38, 250–262. https://doi.org/10.1016/j.wasman.2014.12.012

555 **Figure captions**

556 **Fig 1.** Schematic representation of the experimentation set up

557 **Fig 2.** LBR performances. A : accumulated methane yield, B: methane flow

558 **Fig 3.** Elution curves. A: before SS-AD, B: after 15 days of SS-AD, C: at the end of SS-AD, D: 50% RG
559 before SS-AD for serial and parallel layering

560 **Fig 4.** Elution curves. A: 25% RG, B: 50% RG, C: 75% RG

561 **Fig 5.** Residence time distribution for each experiment. A: Mean residence time, B: Retardation
562 factor

563 **Fig 6.** Hydrodispersive parameters for each experiment. A: the fractions of solid matter filled with
564 stagnant water and B: tracer exchange rate

565

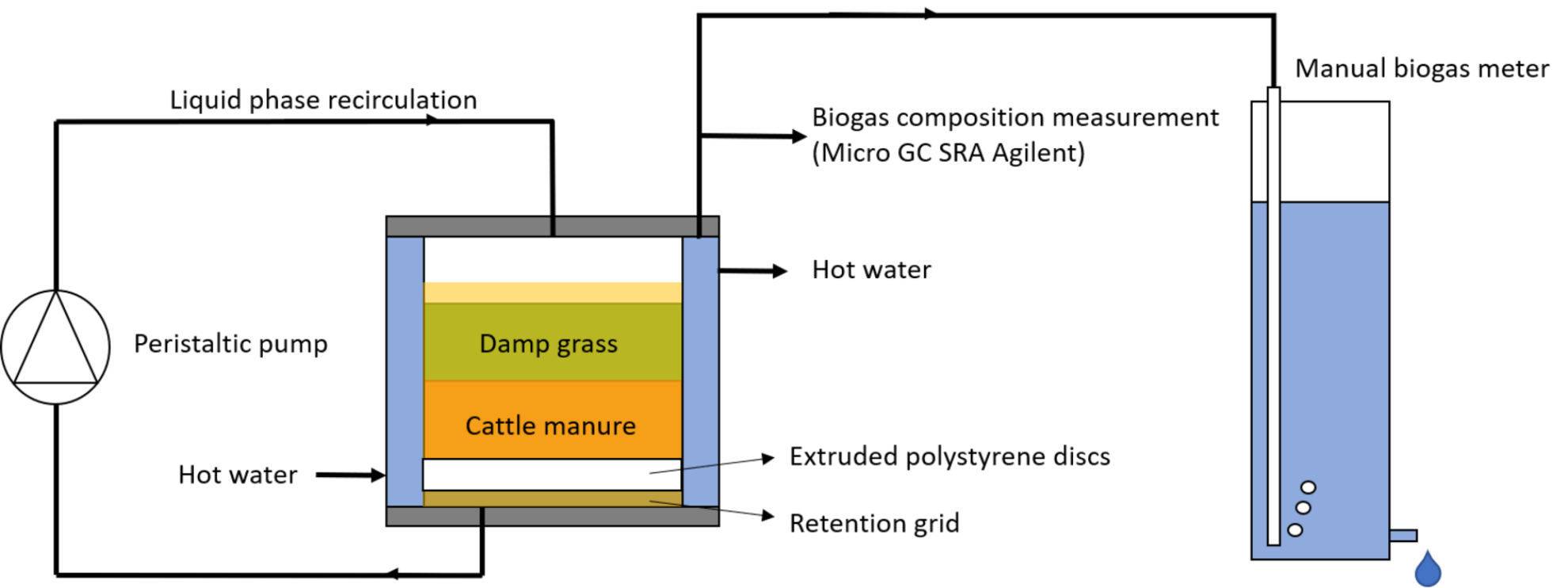
Liquid phase recirculation
Biogas composition measurement
(Micro GC SRA Agilent)
Manual biogas meter
Hot water
Peristaltic pump
Damp grass
Cattle manure
Hot water
Extruded polystyrene discs
Retention grid

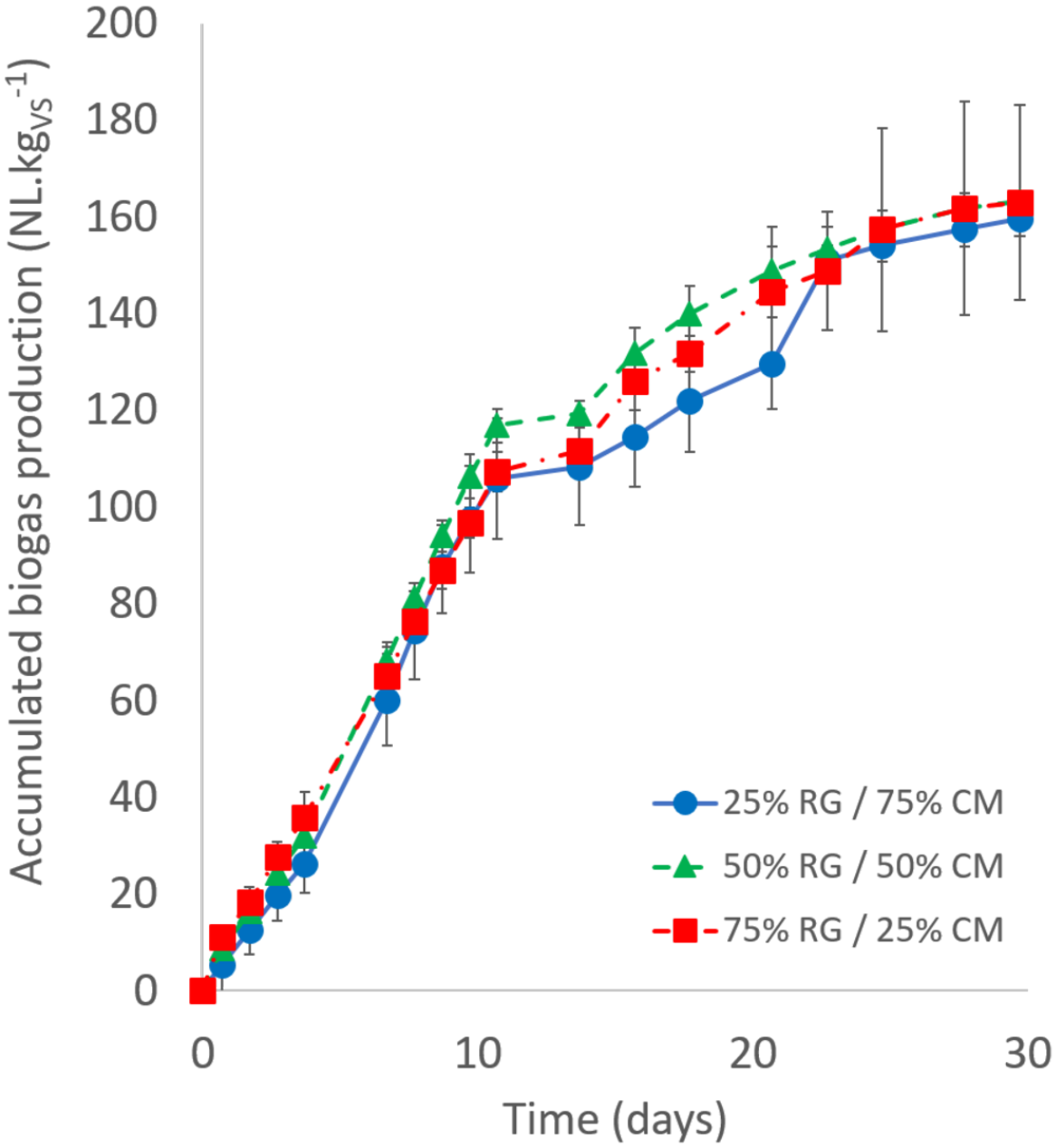
Accumulated biogas production (NL.kg$_{VS}^{-1}$)
200
180
160
140
120
100
80
60
40
20
0
0
10
20
30
Time (days)
25% RG / 75% CM
50% RG / 50% CM
75% RG / 25% CM

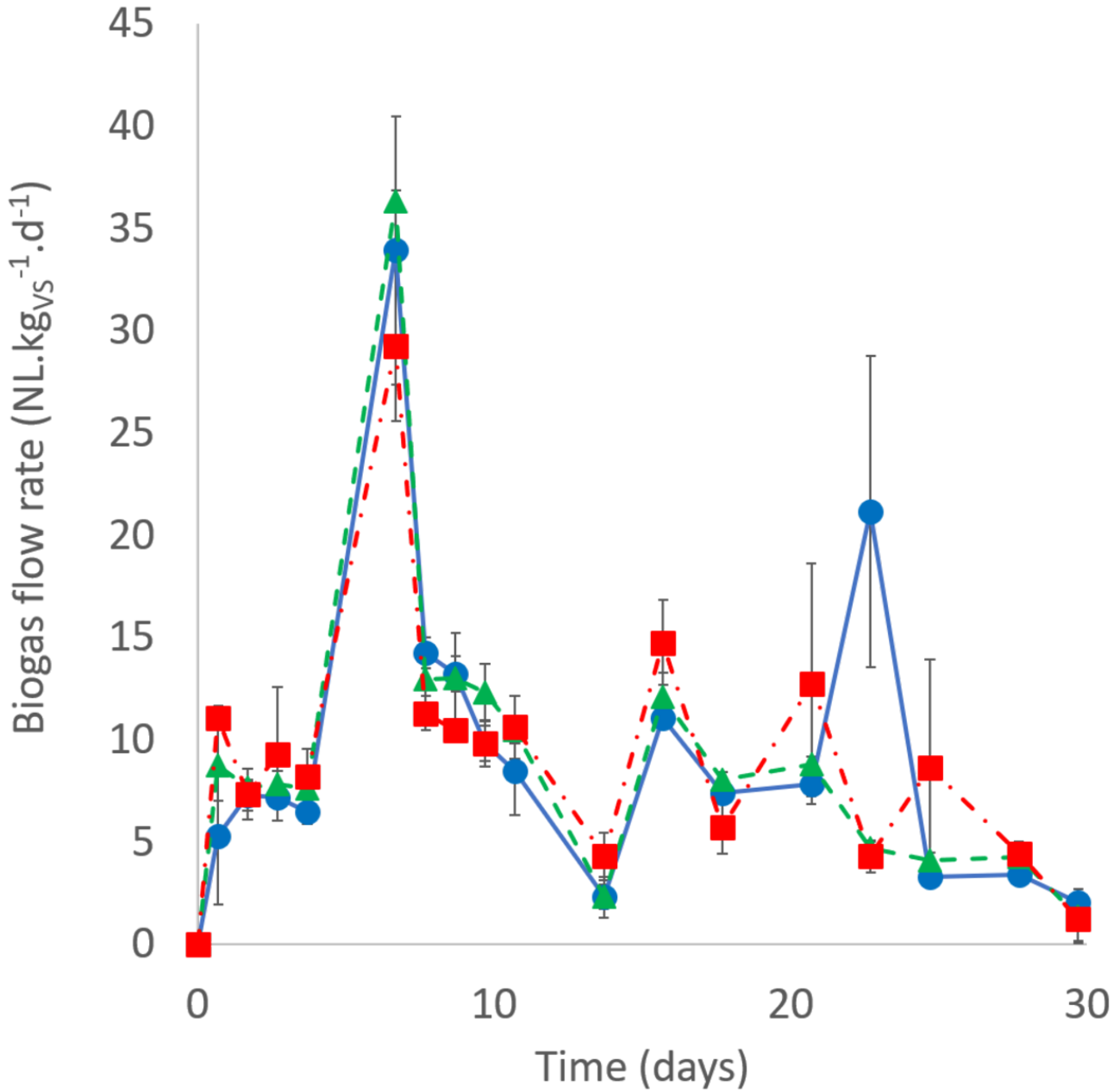
Biogas flow rate (NL.kg$_{VS}^{-1}$.d^{-1})
45
40
35
30
25
20
15
10
5
0
0
10
20
30
Time (days)

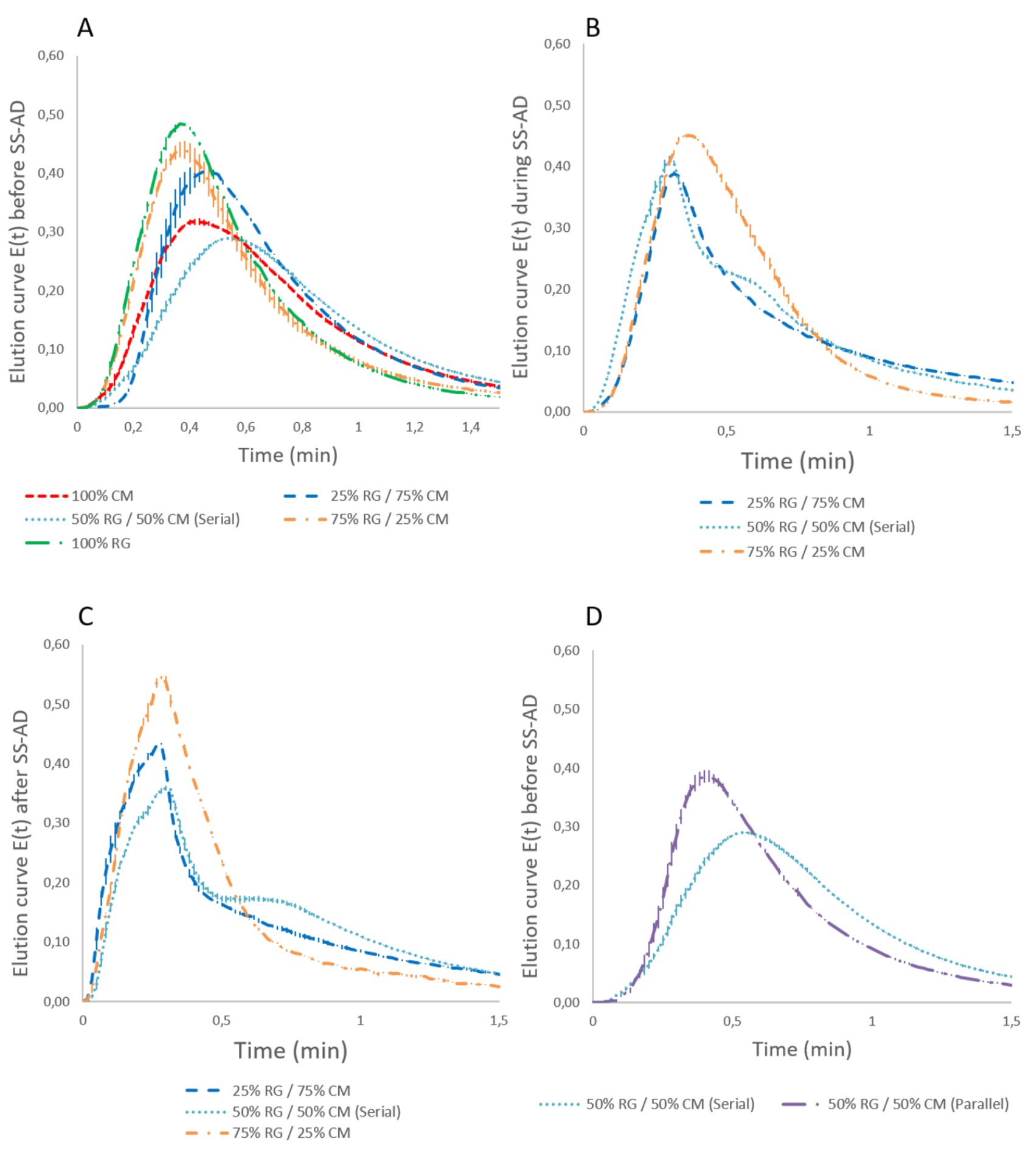
A
Elution curve E(t) before SS-AD
0,60
0,50
0,40
0,30
0,20
0,10
0,00
0
0,2
0,4
0,6
0,8
1
1,2
1,4
Time (min)
100% CM
25% RG / 75% CM
50% RG / 50% CM (Serial)
75% RG / 25% CM
100% RG
B
Elution curve E(t) during SS-AD
0,60
0,50
0,40
0,30
0,20
0,10
0,00
0
0,5
1
1,5
Time (min)
25% RG / 75% CM
50% RG / 50% CM (Serial)
75% RG / 25% CM
C
Elution curve E(t) after SS-AD
0,60
0,50
0,40
0,30
0,20
0,10
0,00
0
0,5
1
1,5
Time (min)
25% RG / 75% CM
50% RG / 50% CM (Serial)
75% RG / 25% CM
D
Elution curve E(t) before SS-AD
0,60
0,50
0,40
0,30
0,20
0,10
0,00
0
0,5
1
1,5
Time (min)
50% RG / 50% CM (Serial)
50% RG / 50% CM (Parallel)

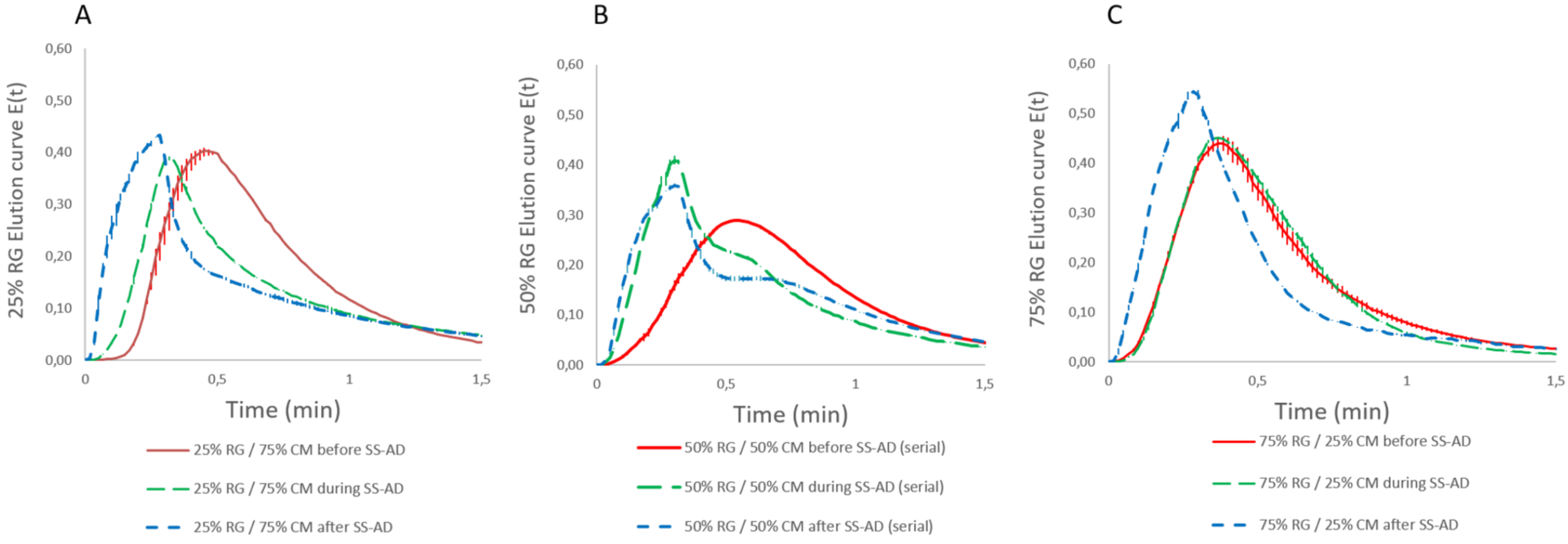
A
B
C
25% RG Elution curve E(t)
50% RG Elution curve E(t)
75% RG Elution curve E(t)
0,60
0,50
0,40
0,30
0,20
0,10
0,00
0
0,5
1
1,5
Time (min)
25% RG / 75% CM before SS-AD
25% RG / 75% CM during SS-AD
25% RG / 75% CM after SS-AD
50% RG / 50% CM before SS-AD (serial)
50% RG / 50% CM during SS-AD (serial)
50% RG / 50% CM after SS-AD (serial)
75% RG / 25% CM before SS-AD
75% RG / 25% CM during SS-AD
75% RG / 25% CM after SS-AD

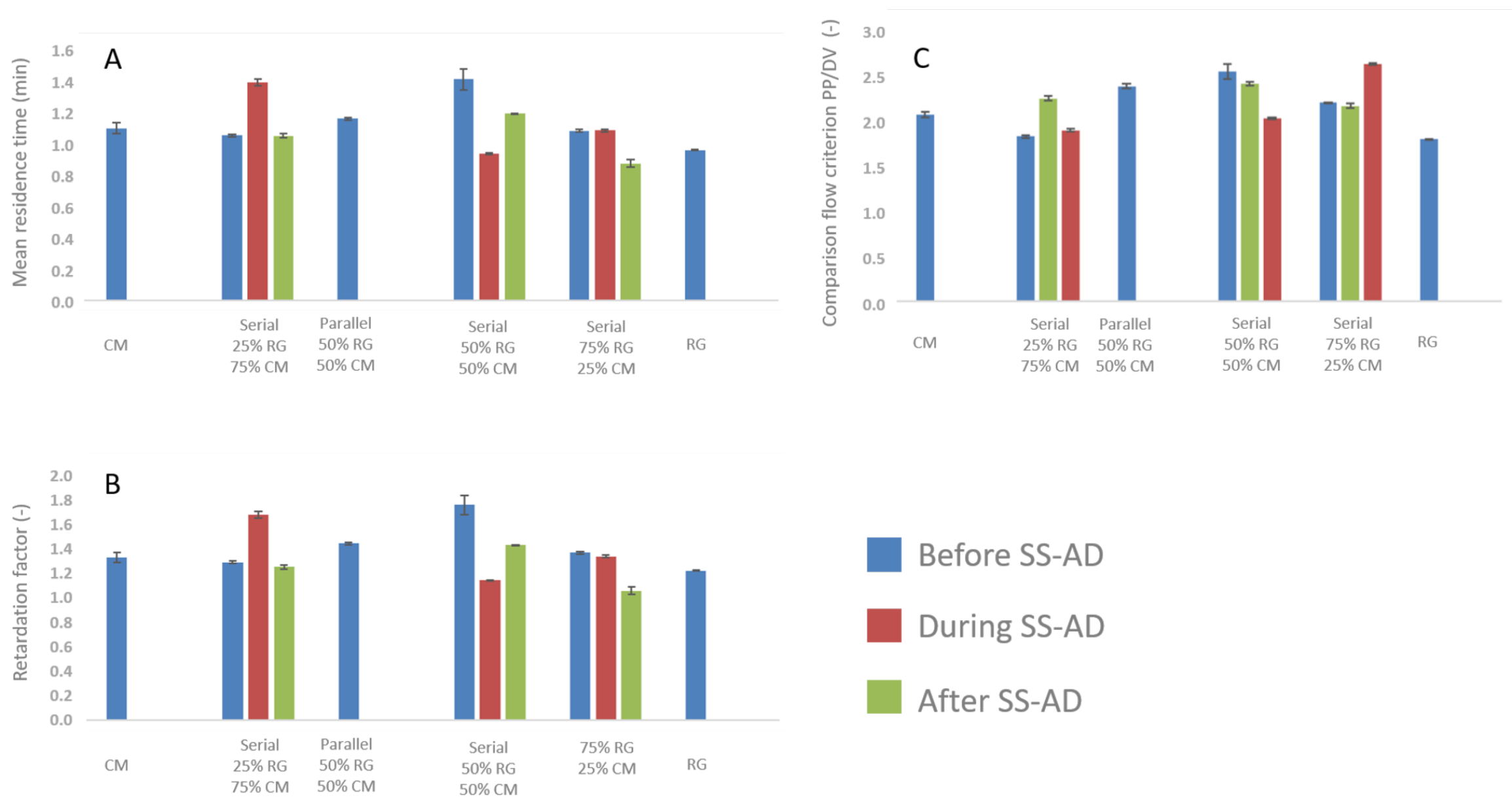
A
Mean residence time (min)
1.6
1.4
1.2
1.0
0.8
0.6
0.4
0.2
0.0
CM
Serial 25% RG 75% CM
Parallel 50% RG 50% CM
Serial 50% RG 50% CM
Serial 75% RG 25% CM
RG
C
Comparison flow criterion PP/DV (-)
3.0
2.5
2.0
1.5
1.0
0.5
0.0
CM
Serial 25% RG 75% CM
Parallel 50% RG 50% CM
Serial 50% RG 50% CM
Serial 75% RG 25% CM
RG
B
Retardation factor (-)
2.0
1.8
1.6
1.4
1.2
1.0
0.8
0.6
0.4
0.2
0.0
CM
Serial 25% RG 75% CM
Parallel 50% RG 50% CM
Serial 50% RG 50% CM
75% RG 25% CM
RG
Before SS-AD
During SS-AD
After SS-AD

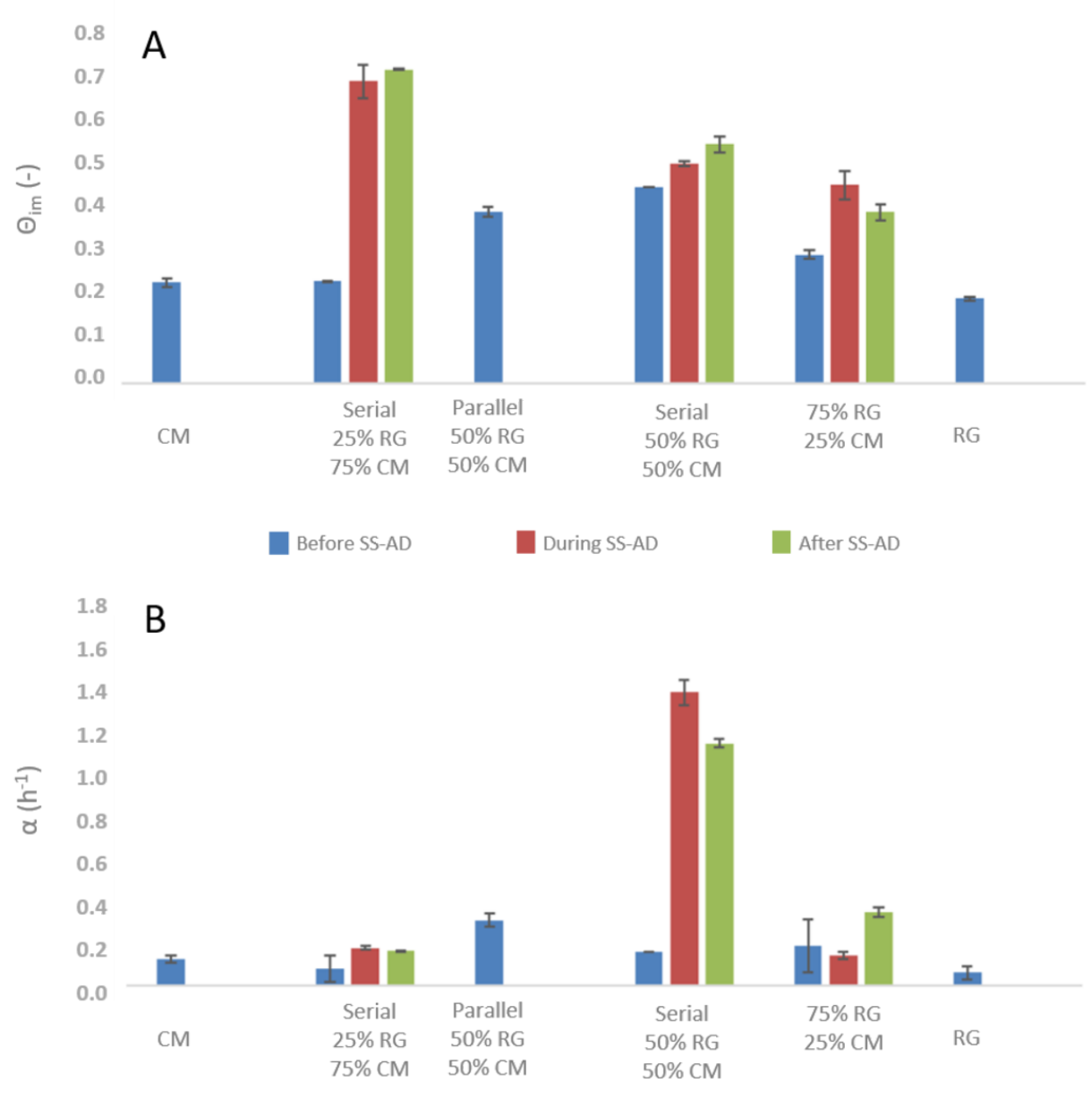
A
Θ_{im} (-)
0.8
0.7
0.6
0.5
0.4
0.3
0.2
0.1
0.0
CM
Serial 25% RG 75% CM
Parallel 50% RG 50% CM
Serial 50% RG 50% CM
75% RG 25% CM
RG
Before SS-AD
During SS-AD
After SS-AD
B
α (h^{-1})
1.8
1.6
1.4
1.2
1.0
0.8
0.6
0.4
0.2
0.0
CM
Serial 25% RG 75% CM
Parallel 50% RG 50% CM
Serial 50% RG 50% CM
75% RG 25% CM
RG

Table 1 Chemical characteristics of inoculum and initial substrates used

	TS ($\%_{FM}$)	**VS** ($\%_{TS}$)	**pH**	**FOS** ($mg.L^{-1}$)	**TAC** ($mg.L^{-1}$)	**BMP** ($NL_{CH4}.kg_{VS}^{-1}$)
Initial CM	19.4 ± 0.36	84.0 ± 0.46	-	-	-	143 ± 12.4
Initial RG	52.1 ± 0.79	61.3 ± 0.44	-	-	-	240 ± 8.95
Initial LM	2.30 ± 0.05	49.9 ± 1.19	7.91 ± 0.04	1695 ± 8.115	10914 ± 309.06	10.4 ± 0.01

Table 2 Leach-bed complexity by Steady-state reactor modeling

Before SS-AD	**Equivalent number of CSTR**
Empty LBR	1
100% CM	7
Serial 75% CM, 25% RG	9
Serial 50% CM, 50% RG	10
Serial 25% CM, 75% RG	11
100% RG	7
Parallel 50% CM, 50% RG	13
During SS-AD	
Serial 75% CM, 25% RG	19
Serial 50% CM, 50% RG	11
Serial 25% CM, 75% RG	13
After SS-AD	
Serial 75% CM, 25% RG	12
Serial 50% CM, 50% RG	9
Serial 25% CM, 75% RG	11

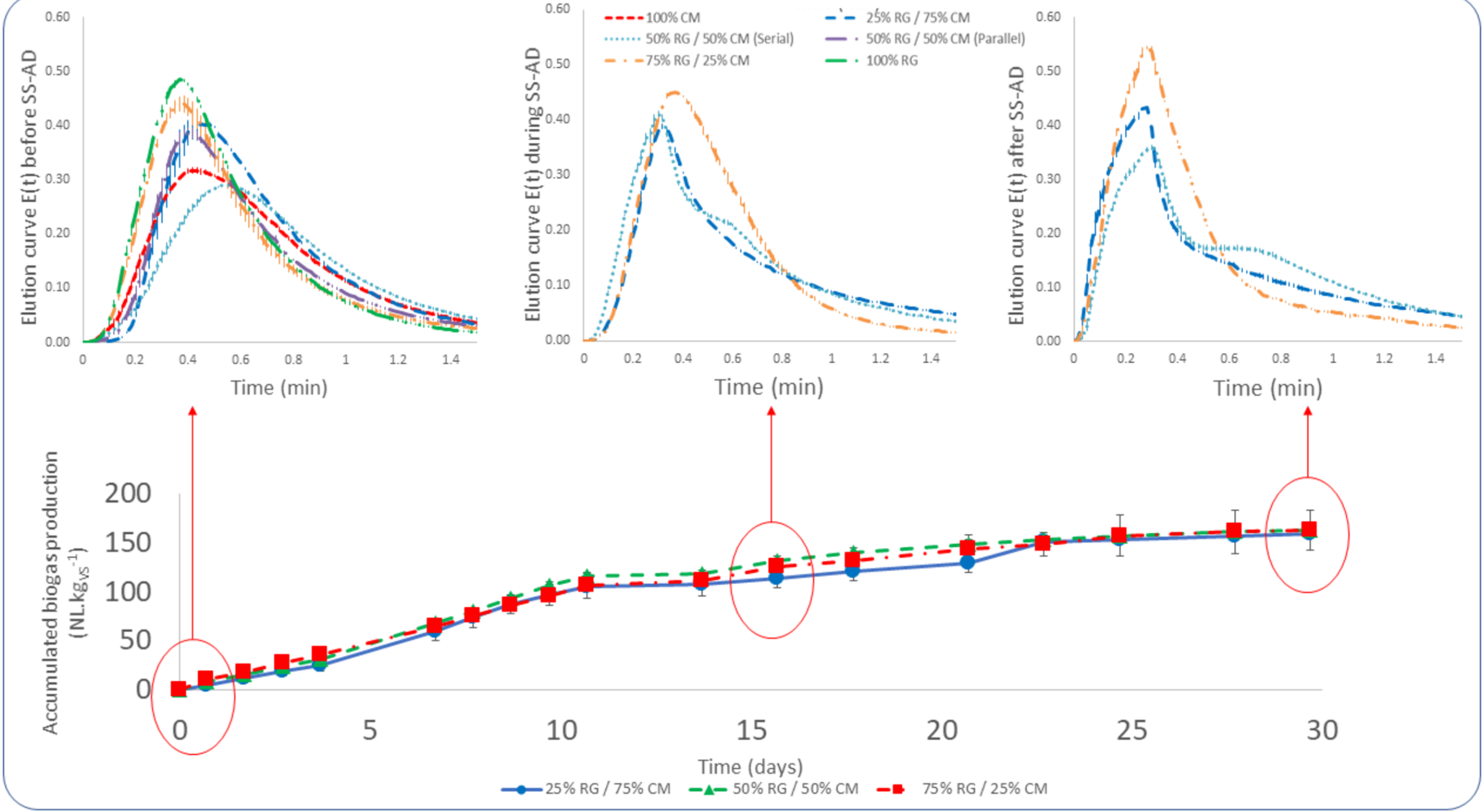
Elution curve E(t) before SS-AD
Time (min)
Elution curve E(t) during SS-AD
100% CM
25% RG / 75% CM
50% RG / 50% CM (Serial)
50% RG / 50% CM (Parallel)
75% RG / 25% CM
100% RG
Time (min)
Elution curve E(t) after SS-AD
Time (min)
Accumulated biogas production (NL.kg$_{VS}^{-1}$)
Time (days)
25% RG / 75% CM
50% RG / 50% CM
75% RG / 25% CM